Structural Competition Involving G-Quadruplex DNA and Its Complement†

Wei Li,‡,# Daisuke Miyoshi,§ Shu-ichi Nakano,‡ and Naoki Sugimoto*,‡,§

High Technology Research Center, and Department of Chemistry, Faculty of Science and Engineering, Konan University, 8-9-1 Okamoto, Higashinada-ku, Kobe 658-8501, Japan

Received January 30, 2003; Revised Manuscript Received June 19, 2003

ABSTRACT: Structural competition between the G-quadruplex, the I-motif, and the Watson−Crick duplex has been implicated for repetitive DNA sequences, but the competitive mechanism of these multistranded structures still needs to be elucidated. We investigated the effects of sequence context, cation species, and pH on duplex formation by the G-quadruplex of $dG_3(T_2AG_3)_3$ and its complement the I-motif of $d(C_3TA_2)_3C_3$, using ITC, DSC, PAGE, CD, UV, and CD stopped-flow kinetic techniques. ITC and PAGE experiments confirmed Watson−Crick duplex formation by the complementary strands. The binding constant of the two DNA strands in the presence of 10 mM Mg^{2+} at pH 7.0 was shown to be 5.28×10^7 M^{-1} at 20 °C, about 400 times larger than that in the presence of 100 mM Na^+ at pH 5.5. The dynamic transition traces of the duplex formation from the equimolar mixture of G-/C-rich complementary sequences were obtained at both pH 7.0 and pH 5.5. Fitting to a single-exponential function gave an observed rate of 8.06×10^{-3} s^{-1} at 20 °C in 10 mM Mg^{2+} buffer at pH 7.0, which was about 10 times the observed rate at pH 5.5 under the same conditions. Both of the observed rates increased as temperature rose, implying that the dissociation of the single-stranded structured DNAs is the rate-limiting step for the WC duplex formation. The difference between the apparent activation energy at pH 7.0 and that at pH 5.5 reflects the fact that pH significantly influences the structural competition between the G-quadruplex, the I-motif, and the Watson−Crick duplex, which also implies a possible biological role for I-motifs in biological regulation.

DNA quadruplexes, which are stabilized by cyclic Hoogsteen hydrogen bonding of four guanines, have generated considerable attention during the past few decades because they are important molecules in drug design (*1*, *2*) and a potential structural motif adopted by the chromosome telomeres (*3*, *4*), immunoglobulin switch regions (*5*−*7*), regulatory regions of oncogenes (*8*), and other biological systems (*9*, *10*). G-quadruplex formation has been shown in vitro to inhibit the elongation of telomerase, which is an enzyme essential for the immortalization of tumor cells (*11*). Recently, a chair-form intramolecular G-quadruplex structure has been proved to suppress the transcriptional activation of the *c-myc* oncogene (*12*). Accompanied by ever-increasing discoveries of G-quadruplex related proteins, such as human DNA topoisomerase I (*13*), BLM (*14*) and WRN (*15*) proteins[1] in the RecQ family of helicases, SV40 large tumor antigen helicase (*16*), and so forth, which not only recognize but also manipulate the formation and the disintegration of G-quadruplexes, biological roles are strongly suggested for this DNA structure in gene regulation. The G-quadruplex is also seen as a promising target for anticancer drug design (*17*). Thus, investigation of the structural competitive mechanism between the G-quadruplex and the Watson−Crick (WC) duplex is fundamental for elucidating how alternative DNA structures with biological implications form.

C-rich strands can, themselves, also form a self-associated structure, the I-motif, intercalated by two parallel duplexes built of hemiprotonated cytidine−cytidine base pairs in antiparallel orientation (*18*−*20*). The detection of a protein from vertebrate nuclear extracts that binds specifically to C-rich sequences (*21*) suggests the possible biological relevance of the I-motif, although the evidence is weaker than that for its role in complementing the G-quadruplex.

A number of small molecular ligands have been shown to have structurally specific recognition for the G-quadruplex and the I-motif. For instance, Hurley's group has reported a series of small ligands that may not only recognize the G-quadruplex through inside intercalation between tetrads (*22*), or outside-stacking interactions (*23*), but also induce transition from the duplex to the quadruplex (*24*). Mergny's group also showed potent small ligands that may stabilize the G-quadruplex and the I-motif, rather than their WC duplex (*25*, *26*). Moreover, interference of the self-associated G-quadruplex or I-motif with formation of the duplex and the triplex has been reported (*27*−*31*). In attempting to understand the effects of this wide variety of structurally

† This work was supported in part by Grants-in-Aid from the Ministry of Education, Science, Sports and Culture, Japan to N.S.

* To whom correspondence should be addressed. Phone: +81-78-435-2497. Fax: +81-78-435-2539. E-mail: sugimoto@konan-u.ac.jp.

‡ High Technology Research Center.

§ Department of Chemistry, Faculty of Science and Engineering.

Present address: School of Chemical Engineering, Tianjin University, Tianjin 300072, P.R.China.

[1] Abbreviations: CD, circular dichroism; UV, ultraviolet spectroscopy; DSC, differential scanning calorimetry; PAGE, polyacrylamide gel electrophoresis; ITC, isothermal titration calorimetry; G-quadruplex, guanine quadruplex; WC duplex, Watson−Crick duplex; BLM protein, Bloom's syndrome protein; WRN protein, Werner's syndrome proteins; MES, 2-morpholinoethanesulfonic acid; Tris, tris(hydroxymethyl)-aminomethane; HPLC, high performance liquid chromatography; pur, purine; pyr, pyrimidine; FITC, Fluorescein isothiocyanate.

10.1021/bi034168j CCC: $25.00
Published on Web 09/17/2003

specific ligands, as well as the transition competition between alternative structures and the WC duplex, there arise some elusive questions about the intrinsic interaction mechanism of the G-quadruplex and its complement I-motif. What is typical of the original interaction between the G-quadruplex and the I-motif under conditions without ligands? What kinds of factors dominate the structural competitive equilibrium? Does the C-rich complement play a role in the structural competition? What are the rates and kinetic mechanisms involved in the formation of a duplex in the mixture of self-associated quadruplexes? To attempt to answer these questions, we studied the interactions of the monomolecular G-quadruplex $dG_3(T_2AG_3)_3$ and its complement I-motif $d(C_3TA_2)_3C_3$ using CD, UV, PAGE, DSC, and ITC. The binding constant of these two sequences showed that the competitive equilibria depend significantly on the cation species and pH. Also, for the first time, kinetic characteristics of the duplex formation in the mixture of the G-quadruplex and the I-motif were investigated using CD stopped-flow techniques. Comparison of the temperature-dependency of the observed rate at pH 7.0 with that at pH 5.5 implied a possible biological role for the I-motif apart from its role as the complement of the G-quadruplex. Kinetic analysis revealed insights into the structural competitive mechanism between the G-quadruplex, the I-motif, and the WC duplex.

MATERIALS AND METHODS

Materials. DNA oligonucleotides shown in Figure 1a were purchased from Espec Oligo Service Corp. (Japan) and then purified by reverse-phase HPLC. The final purity of the oligonucleotides was confirmed to be >99%. Single-strand concentrations were determined by measuring the absorbance (260 nm) at a high temperature using a Hitachi U-3210 spectrophotometer connected to a Hitachi SPR-10 thermoprogrammer. Single-strand extinction coefficients were calculated from mononucleotide and dinucleotide data using a nearest-neighbor approximation (*32*). The different DNA strands were mixed in equimolar amounts, and the total species concentrations were estimated by averaging the extinction coefficients of the single strands. All measurements were performed in a buffer solution consisting of 50 mM MES at pH 7.0 or 50 mM Tris-acetate at pH 5.5. The ionic strength of the buffer was adjusted by the addition of the appropriate salt.

CD Studies. The typical bands in the CD spectra show fundamental characteristics for distinguishing the DNA structure of the G-quadruplex, the I-motif, or the duplex. CD spectra were recorded on a JASCO J-820 spectropolarimeter equipped with a PTC-423L temperature controller. For each sample, at least four spectral scans were accumulated over a wavelength range of 190−350 nm and a temperature range of 0−90 °C in a 0.1 cm path length cell at a scanning rate of 20 nm/min. The scan of the buffer alone was subtracted from the average scan for each sample. CD spectra were collected in units of millidegrees versus wavelength and normalized to the total species concentrations. The cell-holding chamber was flushed with a constant stream of dry nitrogen to avoid water condensation on the cell exterior.

UV Thermal Denaturation Studies. UV thermal denaturation profiles are sensitive to the structural transition of nucleic acids. UV melting curves were recorded with a Hitachi U-3210 spectrophotometer equipped with a Hitachi SPR-10 thermoprogrammer. The water condensation on the cuvette exterior in the low-temperature range was avoided by flushing with a constant stream of dry nitrogen. Melting curves were collected by measuring UV absorbance as a function of temperature. The heating rates were set as 0.5 or 1.0 °C/min (*33*). Prior to the sample experiments, all samples were annealed and degassed by heating the sample cuvette to 90 °C for 10 min and then cooling to 0 °C at 1.0 °C/min. The samples were then allowed to stabilize for about 20 min at the beginning temperature of each heating−cooling cycle. The thermodynamic parameters of the van't Hoff enthalpy ($\Delta H°_{VH}$), the entropy ($\Delta S°$), and the free energy change ($\Delta G°$) for the WC duplex formation were calculated from the melting curves using a curve fitting (*34*, *35*) as well as the reciprocal of the melting temperature, T_m^{-1}, versus $\ln(C_t/4)$ (*36*).

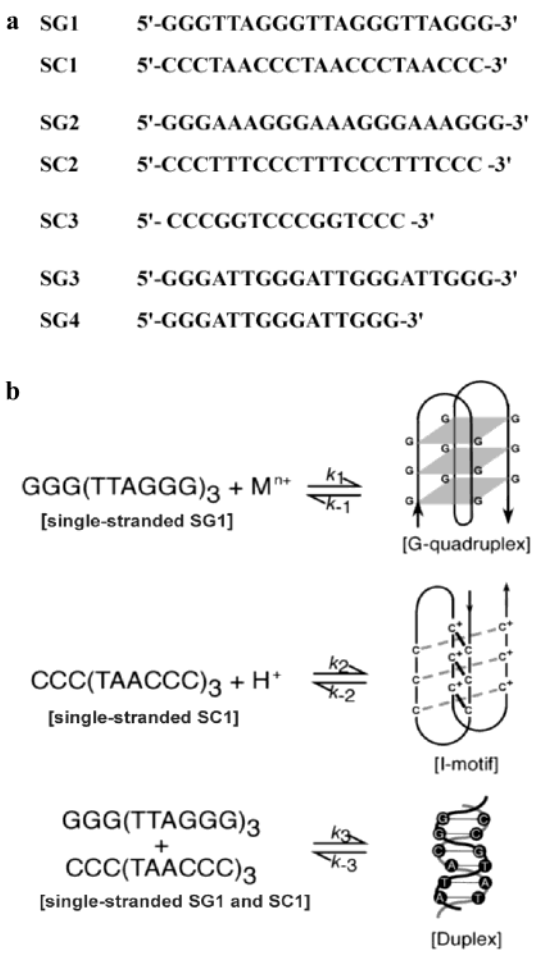

FIGURE 1: (a) Oligonucleotide sequences used in this study. (b) Scheme of the mechanism for duplex formation in the mixture of the G-quadruplex of SG1 and the I-motif of SC1.

of 1 °C/min. The resulting sample versus buffer scans collected for each sample were averaged, the buffer versus buffer baseline was subtracted, and then the scans were normalized by strand concentration and sample volume to obtain the excess heat capacity (ΔC_p). Calorimetrical enthalpy ($\Delta H°_{cal}$) and entropy ($\Delta S°$) were calculated by direct integration of the peak observed in the excess heat capacity profiles (*37*).

PAGE. Native PAGE measurements were carried out using fluorescein-labeled oligonucleotides in 0.089 M Tris-borate buffers (pH 7.0) and 5 mM Tris-acetate buffers (pH 5.5). The same buffer was used in the polymerization of the acrylamide for the relevant gels. The 5′-ends of the oligonucleotide strands were labeled with fluorescein isothiocyanate and annealed by heating the samples to 90 °C for 5 min, cooling to 4 °C, and holding at this temperature for several hours. Electrophoresis was carried out using 20% or 16% acrylamide [29:1 acrylamide/bis(acrylamide)] at 4 V/cm and 4 °C in a total oligonucleotide concentration of 2.0 μM. The fluorescence intensity of each band in the native PAGE images was determined using a Fluor-S MultiImager system (Bio-Rad Laboratories, U.S.A.). The fraction of the duplex, *f*, was then calculated from the band intensities of I_{sG}, I_{sI}, and I_{ds} for the G-quadruplex, the I-motif, and the duplex oligonucleotides, respectively, using the equation $f = I_{ds}/(I_{ds} + I_{sG} + I_{sI})$.

ITC Experiments. ITC measurement can be used to determine the binding constant and the interaction stoichiometry of two complementary sequences. The heat on mixing a G-strand with its complement was measured using a Microcal VP-ITC titration calorimeter. A 250 μL syringe was used for the titratant, and complete mixing was accomplished by stirring with the syringe paddle at 310 rpm. Typically, titration was carried out by injecting 5 μL aliquots of a 30 μM SC1 solution into a 2.0 μM SG1 solution at 10 min intervals at 20 °C for a total of 50 injections. Titration curves were corrected for heat of dilution by injecting the oligonucleotide into the buffer. The resultant titration plot was fitted to a sigmoidal curve by a nonlinear least-squares method using Origin 5.0 (Microcal Software). The binding constant K_a, the stoichiometry *N*, and the enthalpy change $\Delta H°$ were obtained from the curve fitting (*38*). The Gibbs free energy change $\Delta G°$ and the entropy $\Delta S°$ were calculated from the equation $\Delta G° = -RT \ln K_a = \Delta H° - T\Delta S°$.

Stopped-Flow Kinetic Experiments. The CD stopped-flow kinetic measurements were performed using a JASCO J-820 spectropolarimeter equipped with a Unisoku (Japan) two-reservoir cell holder. Temperature was monitored (within ±0.1 °C) using an attached circulating water bath. After rapid mixing of equal volumes of a 50 μM SG1 solution and a 50 μM SC1 solution, the time course of the CD spectrum was recorded in units of millidegrees at the selected wavelength. Data sets from five or six experiments performed under identical conditions were averaged. The averaged data were fitted to appropriate equations using Igor software (WaveMetrics Inc., U.S.A.).

Figure 1b shows a scheme of the duplex formation from a mixture of the G-quadruplex of SG1 and the I-motif of SC1 (herein designated as SG1−SC1). Because the concentration of cation is a large excess over that of the DNA strands, the differential equations describing the time-dependence of [G], [I], and [D] are given in eqs 1, 2, and 3, respectively,

$$\frac{d[G]}{dt} = k_1[SG1] - k_{-1}[G] \quad (1)$$

$$\frac{d[I]}{dt} = k_2[SC1] - k_{-2}[I] \quad (2)$$

$$\frac{d[D]}{dt} = k_3[SG1][SC1] - k_{-3}[D] \quad (3)$$

where [G], [I], and [D] are the concentrations of the G-quadruplex, the I-motif, and the WC duplex, respectively; k_1 and k_{-1}, and k_2 and k_{-2} are the folding rate constant and the unfolding rate constant for the G-quadruplex and for the I-motif, respectively; k_3 is the association rate constant; and k_{-3} is the dissociation rate constant for the WC duplex formation.

Association of the SG1 and the SC1 leading to duplex formation gave a decrease in the CD intensity at the wavelength where the typical bands of the G-quadruplex and the I-motif were located, as well as an increase in the CD intensity at 265 nm, corresponding to the WC duplex. Because the association rate of the duplex is fast and the I-motif is less stable at pH 7.0, the observed rates in the mixture of the G-quadruplex and the I-motif should correspond to the rate-limiting step, the dissociation of the single-stranded G-quadruplex. When the intermediates are unstable and are expected to be present in low amounts compared with those of the structured single-strand DNA reactants or the WC duplex product, we can rewrite eq 1 as pseudo-first-order kinetics, eq 4, where θ indicates the CD intensity,

$$\frac{d\theta}{dt} \propto \frac{d[G]}{dt} = k_{-1}[G]\left(\frac{k_1[SG1]}{k_{-1}[G]} - 1\right) \approx -k_{-1}[G] \quad (4)$$

RESULTS AND DISCUSSION

Conditions Forming the WC Duplex from Structured DNAs. Formation of the WC duplex by the DNA strands, SG1 and SC1, and SG2 and SC2, was investigated. As shown in Figure 1a, SG1 and SC1 are the model oligonucleotides derived from a tandem repetitive G-/C-rich sequence of the human telomeres (*39*). The contiguous guanine strand forms planar G-quartets with loops (Figure 1b). Sequences of SG1 and SG2, that is, $dG_3(T_2AG_3)_3$ and $dG_3(A_3G_3)_3$, are similar to each other except for the two-residue replacement from T to A in the loop region, and vice versa for the complementary C-rich sequences of SC1 and SC2. Our previous study revealed that cation species and pH might affect duplex formation in the mixture of an intramolecular G-quadruplex of SG1 and an I-motif of SC1 (*40*). To clarify the mechanism of the duplex formation by the structured DNA strands, we first performed isothermal titration calorimetry (ITC) on the formation of the WC duplex by SG1 and SC1.

Figure 2a shows the ITC profiles for the association of SG1 with SC1. Reactions in 10 mM Mg^{2+} and in 100 mM Na^+ at pH 7.0 produced substantial heat while titration in 100 mM Na^+ at pH 5.5 gave less. Thermodynamic parameters were calculated from the titration plots as a function of the molar ratio of the two DNA strands, although

Table 1: Thermodynamic Parameters for the Duplex Formation by SG1 and SC1 at 20 °C Obtained from the ITC and DSC Measurements

cation	pH	N	K_a (M^{-1})	K_a (relative)	$\Delta H°_{ITC}$ (kcal/mol)	$\Delta G°_{ITC}$ (kcal/mol)	$\Delta H°_{cal}$[e] (kcal/mol)
Na^+[a]	7.0	0.80 ± 0.01	$(1.32 \pm 0.2) \times 10^7$	1.0	-95.0 ± 1.8	-9.52 ± 1.4	-61.8 ± 2.6
Na^+[b]	5.5	nd[d]	$(2.90 \pm 2.0) \times 10^5$	~0.01	nd[d]	nd[d]	-56.6 ± 2.0
Mg^{2+}[c]	7.0	0.82 ± 0.01	$(5.28 \pm 0.8) \times 10^7$	4.0	-135 ± 2.0	-10.3 ± 1.5	-79.1 ± 2.4

[a] 100 mM Na^+ (50 mM MES). [b] 100 mM Na^+ (50 mM Tris-acetate). [c] 10 mM Mg^{2+} (50 mM MES). [d] Thermodynamic parameters cannot be determined accurately because of weak interactions. [e] Calorimetric enthalpy obtained from DSC.

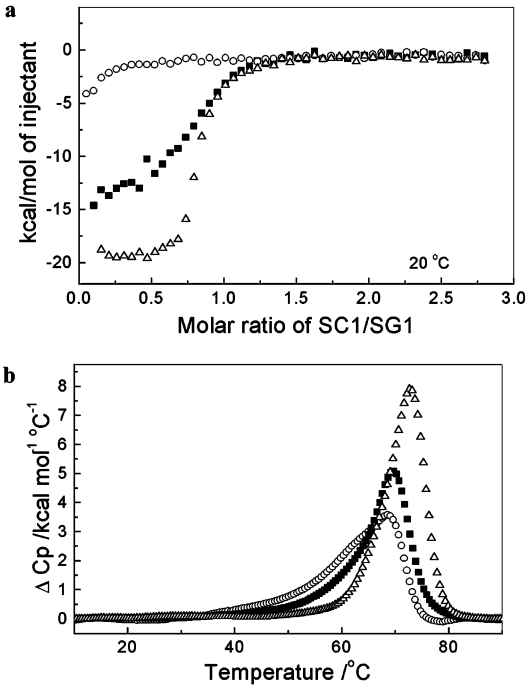

FIGURE 2: (a) ITC profiles for the duplex formation by mixing the G-quadruplex of SG1 with the I-motif of SC1 at 20 °C. The titration plots against the molar ratio of SC1/SG1 were done in 100 mM Na^+ (pH 5.5, ○), 100 mM Na^+ (pH 7.0, ■), and 10 mM Mg^{2+} (pH 7.0, △). (b) DSC profiles for the double-stranded SG1−SC1 in 100 mM Na^+ (pH 5.5, ○), 100 mM Na^+ (pH 7.0, ■), and 10 mM Mg^{2+} (pH 7.0, △).

thermodynamic parameters at pH 5.5 could not be derived because of the lower ITC response. A typical ITC profile for the interaction between SG1 and SC1 in 100 mM Na^+ at pH 5.5 and 20 °C was showed in Figure S1 in the Supporting Information. Table 1 summarizes the thermodynamic parameters for SG1−SC1 duplex formation obtained from the ITC experiments. At pH 7.0, the binding stoichiometry between SG1 and SC1 was approximately 1:1 in the presence of magnesium ion and also in the presence of sodium ion. This observation supports the preference for duplex formation at pH 7.0 in the mixture of structured DNAs, that is, the G-quadruplex of SG1 and the I-motif of SC1. The K_a at 10 mM Mg^{2+} (pH 7.0) was 4 times larger than that at 100 mM Na^+ (pH 7.0) and about 100 times larger than that at 100 mM Na^+ (pH 5.5), which indicates that acidic pH lessens duplex formation. The magnitude of the negative $\Delta H°_{ITC}$ value in the magnesium buffer was 1.4 times that in the sodium buffer at pH 7.0. Both results are consistent with our previous observation that magnesium ion stabilizes the WC duplex but destabilizes the G-quadruplex (*40*). Moreover, according to the DSC results for the double-stranded system SG1−SC1, the excess heat capacity profile clearly shows a deterioration of WC duplex formation in 100 mM Na^+ at pH 5.5 (Figure 2b), and the calorimetric enthalpy obtained from the DSC profiles also shows destabilization of the duplex at acidic pH (Table 1). Figure 2b indicated that the DSC profile of the double-stranded SG1−SC1 at 100 mM Na^+ and pH 7.0 was not a standard symmetric band corresponding to only one simple structural transition, but a complex band with a broad base and a narrow peak. At 10 mM Mg^{2+} and pH 7.0 the DSC profile showed a relatively symmetric curve compared with that at 100 mM Na^+, because the magnesium ion made the G-quadruplex destabilized. As pH was lowered to 5.5, the I-motif of SC1 was stable and the DSC profile at 100 mM Na^+ and pH 5.5 appeared as a more complex band with a larger width at its bottom. This one-peak complex DSC profile further confirmed that the structural transitions of the single-stranded SG1 and SC1 were associated with that of the duplex SG1−SC1. On the other hand, Scaria and Shafer have reported a similar one-peak complex DSC profile for another complementary sequences of $d(G_3A_4G_3)\cdot d(C_3T_4C_3)$ (*41*).

An electrophoretic mobility shift assay for the two-stranded SG1−SC1 system gave results in accord with the ITC and DSC data. Figure 3a and b shows the native PAGE images for the mixture of SG1 and SC1 with various molar ratios in 100 mM Na^+ buffer at pH 5.5, and in 10 mM Mg^{2+} at pH 7.0. At 100 mM Na^+ and pH 5.5, each lane revealed a dominant band assigned to the WC duplex competing with the unimolecular structures of the G-quadruplex and the I-motif. As for the case in 10 mM Mg^{2+} and pH 7.0, there still existed a tiny shadow area around the position of self-associated unimolecular structures besides the duplex band in the equimolar mixture of SG1 and SC1. Figure 3c presented plots of the fraction of the duplex determined from the PAGE images as a function of the molar ratio of SC1/SG1 under different buffer conditions. At pH 7.0 the fraction of the WC duplex reached a maximum as the molar ratio of SC1/SG1 approached unity, whereas the duplex fraction at pH 5.5 showed less dependence on the ratio of SC1/SG1. This result is consistent with the relative trend of interaction between SG1 and SC1 under different buffer conditions, as observed by ITC. The decrease in the fraction of the WC duplex as pH decreased from 7.0 to 5.5 suggests that the I-motif formation of SC1 at acidic pH plays a substantial role in the structural transition toward the duplex. The structural transition in the two-strand SG1−SC1 system was assumed to be as illustrated in Figure 1b.

As a contrastive two-stranded system, duplex formation from a G-rich strand SG2 and its complementary C-rich sequence SC2 was also investigated. The native PAGE images showed only one band for an equimolar mixture of SG2 and SC2 in the presence of magnesium ion as well as in the presence of sodium ion (data not shown), which indicated that the WC duplex overwhelmed the self-associating structures of the single strands in the equimolar mixture of SG2−SC2. Intriguingly, CD spectra for the SG2−SC2

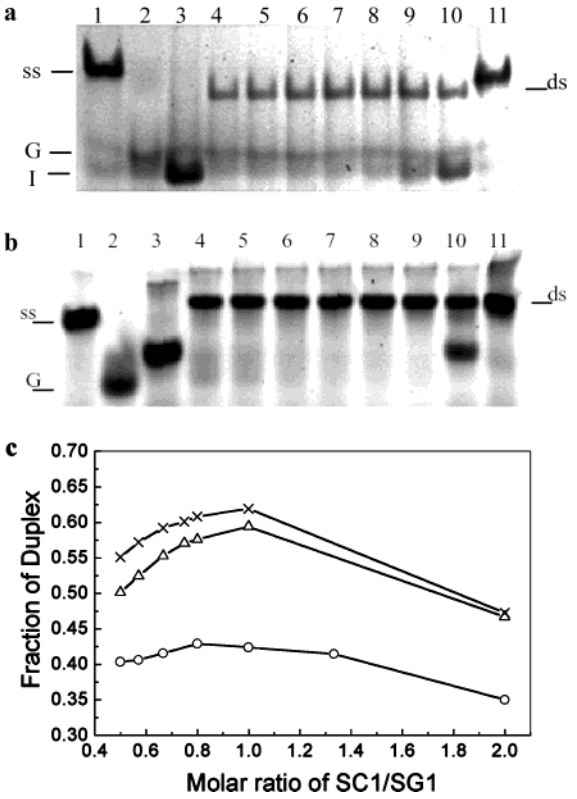

FIGURE 3: (a) Native 20% PAGE images of the double-stranded system in 100 mM Na^+ buffer (pH 5.5). Lane 1 contains the single-stranded marker (T_{21}). Lanes 2 and 3 contain SG1 and SC1, respectively. Lanes 4−10 contain the mixture of SG1/SC1 at molar ratios of 2:1, 7:4, 6:4, 5:4, 1:1, 3:4, and 1:2, respectively. Lane 11 contains the double-stranded marker (A_{21}/T_{21}). The positions of the single strand (ss), the duplex (ds), the G-quadruplex (G), and the I-motif (I) are indicated. (b) Native 20% PAGE images of the double-stranded system in 10 mM Mg^{2+} buffer (pH 7.0). Lane 1 contains the single-stranded marker (T_{21}). Lanes 2 and 3 contain SG1 and SC1, respectively. Lanes 4−10 contain the mixture of SG1/SC1 at molar ratios of 2:1, 7:4, 6:4, 4:3, 5:4, 1:1, and 1:2, respectively. Lane 11 contains the double-stranded marker (A_{21}/T_{21}). (c) Plots of duplex fraction versus the molar ratio of SC1/SG1 obtained by native PAGE in 100 mM Na^+ at pH 5.5 (○), 100 mM Na^+ at pH 7.0 (△), and 10 mM Mg^{2+}at pH 7.0 (×).

system suggest that triplex formation occurred as the molar ratio of SC2/SG2 increased from 1.0 to 2.0 (Figure 4). For the SC2−SG2−SC2 system at 10 mM Mg^{2+} (pH 5.5), a larger negative peak at 213 nm and a positive peak at 284 nm implied triplex formation through the triplet base pairings of C^+*G•C (*42*). The native PAGE images confirmed triplex formation in the two-strand SG2−SC2 system by targeting the SG2−SC2 duplex with an excess amount of SC2 (Figure S2 in the Supporting Information). Similarly, Scaria and Shafer also reported a triple helix formation by a duplex of $dG_3(A_4G_3)_3$•$d(C_3T_4)_3C_3$ with $d(C_3T_4)_3C_3$ at pH 5.3 (*41*). Unlike the case of the SG2−SC2 system, we cannot discern triplex formation for the SG1−SC1 system by targeting the SG1−SC1 duplex with either additional SG1 or SC1 (Figures 2a and 3a). CD spectra of the SG1−SC1 duplex and the SC1−SG1−SC1 triplex were similar (Figure 4), indicating less triplex formation in the mixture of SC1−SG1 and SC1 even at 10 mM Mg^{2+} and pH 5.5.

The stabilities of the SG1−SC1 and SG2−SC2 duplexes were compared using the thermodynamic parameters determined from the UV thermal denaturation profiles, as listed in Table 2. Taking into consideration the effect of the

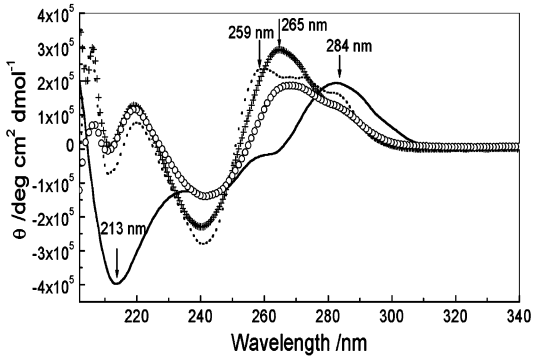

FIGURE 4: CD spectra in 10 mM Mg^{2+} buffer at 0 °C for the double-stranded system of SG2−SC2 with molar ratios for SC2/SG2 of 1.0 (pH 7.0, dotted line) and 2.0 (pH 5.5, solid line), together with those for the SG1−SC1 system with molar ratios for SC1/SG1 of 1.0 (pH 7.0, +) and 2.0 (pH 5.5, ○).

imperfect duplex formation (as shown in Figure 3), the absolute values of the entropy would have a relative increment of 0.4% at 100 mM Na^+ and pH 7.0, 0.3% at 10 mM Mg^{2+} and pH 7.0, and 0.5% at 100 mM Na^+ and pH 5.5, respectively. Consequently, the variation of the entropy made the corresponding free energy change have a relative decrease of 2.3% at 100 mM Na^+ and pH 7.0, 1.3% at 10 mM Mg^{2+} and pH 7.0, and 3.0% at 100 mM Na^+ and pH 5.5, respectively. Therefore, it is reasonable to neglect the effect of the duplex fraction on the values of thermodynamic parameters (as proved in the Supporting Information). The large disparities of the enthalpy and the entropy obtained from two different analysis methods, that is, using the plots of melting temperature against the species concentrations and using a nonlinear least-squares fitting method, respectively, indicated that the double-stranded system was not a two-state-model system and the partial association between the complementary sequences indeed affected the properties of the system. The free energy change indicated that the SG2−SC2 duplex was less stable than the SG1−SC1 duplex in the presence of magnesium ion, although it was in the SG1−SC1 system that a distinct structural competition was observed between the G-quadruplex, the I-motif, and the duplex. Why is it that the less stable SG2−SC2 duplex can overwhelm the formation of the G-quadruplex and the I-motif? What are the important factors that influence the competitive equilibria besides the thermodynamic stability of the duplex? To clarify these questions, we investigated the self-associated structure of each single strand and certainly proposed interactions of a third strand toward the SG1−SC1 duplex target.

Effect of the Loop Sequences in the G-Quadruplex and the I-Motif on the Structural Competition. The CD spectra in Figure 5 reflect clear structural variations for the G-quadruplexes that result from residue replacement in the loop region. Generally, an antiparallel G-quadruplex is characterized by a positive band at 295 nm and a negative band near 265 nm (*44*), while a parallel G-quadruplex has a peak near 270 nm and a negative band around 240 nm (*45*, *46*). CD spectra in Figure 5a indicated that SG1 formed an antiparallel G-quadruplex while SG2 seemed to form a parallel G-quadruplex. Previously we proved that the G-quadruplex of SG1 was an intramolecular structure (*40*); however, CD melting curves for SG2 showed a biphasic transition with melting temperatures of 21 and 47 °C, lower than that of

Table 2: Thermodynamic Parameters for the SG1−SC1and the SG2−SC2 Duplexes Obtained from UV Melting Curves

	calc using the plots of the reciprocal of the melting temp in the function $\ln(C_t/4)$			calc using a nonlinear least-squares fitting method		
	$\Delta H°_{vH}$ (kcal/mol)	$\Delta S°$ (cal/(mol °C))	$\Delta G°_{37}$ (kcal/mol)	$\Delta H°_{vH}$ (kcal/mol)	$\Delta S°$ (cal/(mol °C))	$\Delta G°_{37}$ (kcal/mol)
			SG1−SC1			
100 mM Na^+ (pH 5.5)	-73.8 ± 5.7	-198 ± 12	-12.5 ± 0.9	-50.4 ± 1.5	-129 ± 4.5	-10.4 ± 0.2
100 mM Na^+ (pH 7.0)	-104 ± 5.7	-282 ± 16	-17.0 ± 1.1	-127 ± 6.4	-347 ± 19	-18.9 ± 0.6
10 mM Mg^{2+} (pH 7.0)	-223 ± 6.6	-620 ± 19	-30.5 ± 0.9	-120 ± 5.4	-325 ± 16	-19.7 ± 1.0
			SG2−SC2			
10 mM Mg^{2+} (pH 7.0)	-167 ± 8.3	-456 ± 23	-25.9 ± 1.1	-77.7 ± 3.4	-202 ± 10	-15.0 ± 0.4

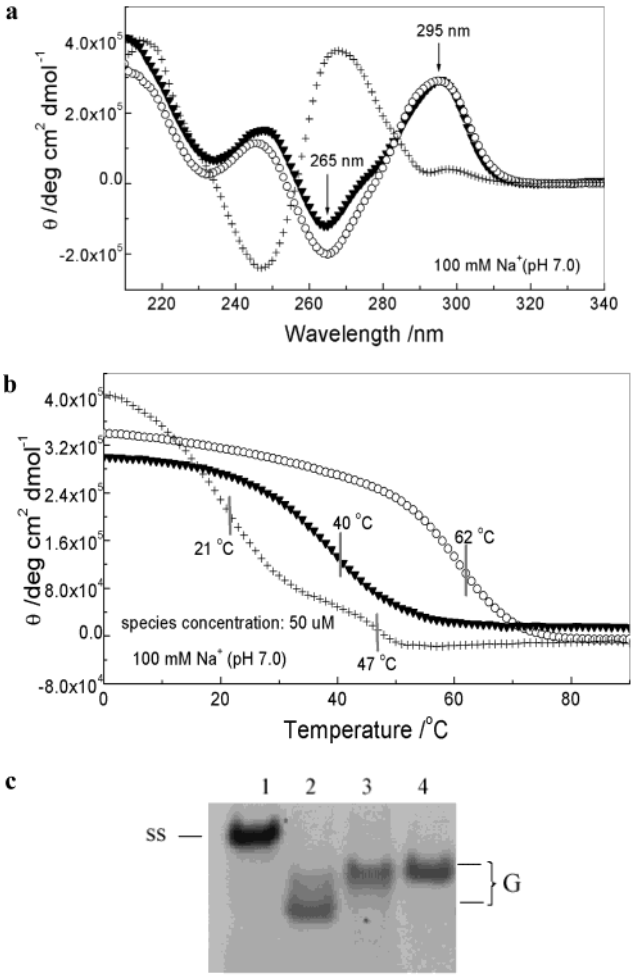

FIGURE 5: Characterization of the single-stranded G-rich oligonucleotides. (a) CD spectra in 100 mM Na^+ at pH 7.0 for SG1 (○), SG2 (+), and SG3 (▼). (b) CD melting curves of SG1 at 295 nm (○), SG2 at 268 nm (+), and SG3 at 295 nm (▼) in 100 mM Na^+ at pH 7.0. (c) Native PAGE images of G-strands in 100 mM Na^+ buffer (pH 7.0) at 4 V/cm and 4 °C. Lanes 1−4 contain the single-stranded marker (T_{21}), SG1, SG2, and SG3, respectively. The positions of the single strand (ss) and G-quadruplex (G) are indicated.

SG1 (62 °C) in the same buffer (Figure 5b). The melting temperature of the low-temperature transition for SG2 was dependent on the DNA concentration, whereas that of the high-temperature transition was independent of the concentration (data not shown). We have done DSC experiments for SG2 at higher sequence concentrations, of which the maximal value is up to 110 μM. The DSC profiles also reflected the existence of the low-temperature transition as well as the high-temperature transition (data not shown). However, the native PAGE image in Figure 5c only showed one band for SG2, whose electrophoretic mobility was lower than that of SG1. As far as the structural polymorphism of repetitive polypurine sequences is concerned, it is suggested that SG2 formed not only an intramolecular G-quadruplex but also somewhat intermolecular structures (*46*−*50*), which needs to be clarified by further investigations.

The G-rich oligomer SG3 contained the same base context as SG1 but in the opposite strand orientation. Like SG1, SG3 had CD spectra typical of an antiparallel G-quadruplex in the presence of sodium ion. However, the transition temperature of the SC3 G-quadruplex (40 °C) was much lower than that of SG1, as was the electrophoretic mobility of SG3 (Figure 5).

Both SG2 and SG3 formed less stable G-quadruplexes than SG1. Therefore, the proposed interaction between SG2 or SG3 and the duplex SG1−SC1 was investigated in terms of the antiparallel pur*pur·pyr triplets of the triplex, including T*A·T, A*A·T, and G*G·C (*42*, *51*). Additionally, the G-rich strand SG4 was also studied as a third strand because of its inability to form an intramolecular G-quadruplex. CD spectra of the related three-strand systems showed no significant differences from that of the duplex SG1−SC1 in 100 mM Na^+ (pH 7.0), except for two broad peaks around 265 and 295 nm in the SG3 and SG1−SC1 mixture (Figure S3a in the Supporting Information). Although UV melting curves for these three-strand systems did not show a biphasic transition that suggested formation of a stable triplex, there was a decrease in the transition temperature that resulted from the interaction between the SG1−SC1 duplex and the third G-rich strand, especially SG3 (Figure S3b in the Supporting Information). To resolve the interaction between SG3 and the SG1−SC1 duplex, we investigated the thermal denaturation of the two-strand SG3−SC1. The thermodynamic parameters for SG3−SC1 were determined as $\Delta H°_{VH} = -130$ kcal mol^{-1}, $\Delta S° = -391$ cal mol^{-1} °C^{1-}, and $\Delta G°$ (at 37 °C) $= -8.81$ kcal mol^{-1} in 10 mM Mg^{2+} buffer (pH 7.0), using the plots of melting temperature against the species concentrations (Figure S4 in the Supporting Information). On comparison with thermodynamic parameters of the SG1−SC1 duplex, listed in Table 2, it is obvious that the SG1−SC1 duplex is much more stable than the SG3−SC1 duplex. The interference of SG3 with the stable SG1−SC1 duplex implies the possibility of invasion of the telomeric double-stranded part by the G-strand extension.

The C-rich oligomers SC2 and SC3 were studied as the third strand targeting the of SG1−SC1 duplex at acidic pH to form triplet base pairs in a pyr*pur·pyr triplex, including T*A·T, C^+*G·C, and the relatively stable mismatched triplet base pair G*T·A (*42*, *51*). The sequence of SC2 differed

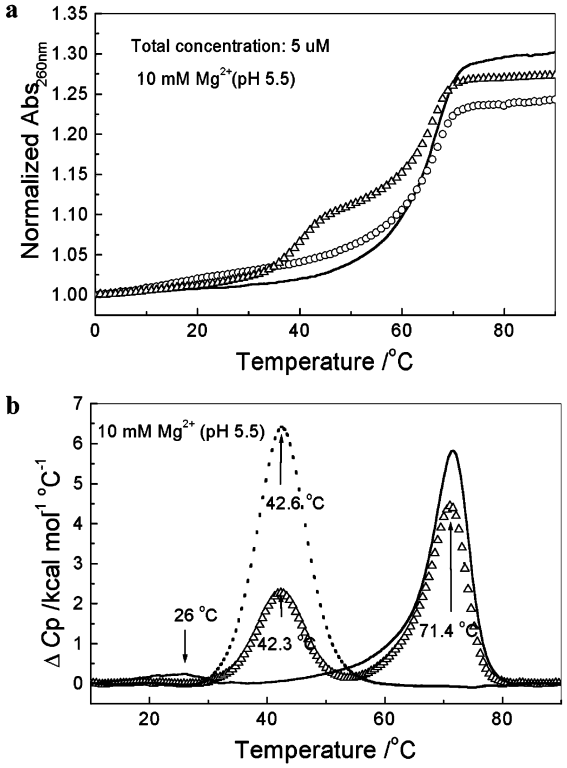

FIGURE 6: (a) UV melting curves for the three-stranded systems targeting the duplex SG1·SC1 (solid line) in 10 mM Mg^{2+} at pH 5.5, with a third strand of SC2 (△) or SC3 (○). (b) Excess heat capacity profiles vs temperature for the three-stranded SC2−SG1−SC1 (△) and SC3−SG1−SC1 (solid line) and for the single-stranded SC2 (dotted line) in 10 mM Mg^{2+} at pH 5.5.

from SC1 only in the two-residue replacements from A to T in the loop region. As pH decreased from 7.0 to 5.5, a distinct red-shift of the positive peak from 276 to 288 nm occurred in CD spectra for SC1, which can be attributed to the pH-dependence of the I-motif structure (*52*). In contrast, SC2 showed a slight red-shift of the CD bands as pH decreased (Figure S5 in the Supporting Information). At pH 5.5, the mobility of SC2 in the PAGE was lower than that of SC1, while the transition temperature of SC2 (42 °C) was slightly higher than that of SC1 at 39 °C (Figure S6 in the Supporting Information). This suggests that residue replacement in the loop may not influence the stability of the I-motif as significantly as that of the G-quadruplex.

Figure 6a shows the UV melting curves of the three-stranded systems SC2−SG1−SC1 and SC3−SG1−SC1 at 10 mM Mg^{2+} and pH 5.5. A clear biphasic transition appeared in the thermal denaturation profile of the mixing system of SC2 and SG1−SC1, in which the lower transition temperatures were independent of the species concentration, unlike the concentration-dependence of the higher transition temperatures. Additionally, comparing the excess heat capacity profile of the single-stranded SC2 with that of the three-stranded (as shown in Figure 6b) suggests that in the three-strand SC2−SG1−SC1 system the lower-temperature structural transition was due to dissociation of the self-associated I-motif formed by single-strand SC2 itself, and the higher-temperature transition corresponds to dissociation of the SG1−SC1 duplex. As for the other three-strand system, SC3−SG1−SC1, both the UV melting curves and a small peak at 26 °C in the DSC profile indicated less triplex formation.

These experimental results demonstrate that it is difficult for the heteropurine/pyrimidine, SG1−SC1, to obtain a stable triplex formation according to the well-known and distinct patterns of triplexes, that is, pyr × pur·pyr and pur × pur·pyr triplexes. However, the data enlighten us on the important influence of the loop residues on structural competition between the G-quadruplex, the I-motif, and the duplex. Combined with the results of duplex formation in the mixture of the G-quadruplex and the I-motif including SG1−SC1 and SG2−SC2, this reveals that the loop residue context of the DNA sequence plays a role, not only in the stability of the self-associated G-quadruplex and the I-motif but also in formation of the duplex and in the structural competitive equilibria. Consequently, the loop residue context might be an important factor determining the conservative property of the telomere DNA sequences in the long process of evolution.

CD Stopped-Flow Kinetics and Rate-Limiting Step of the Duplex Formation. The kinetics of the interaction between the SG1 G-quadruplex and the SC1 I-motif was measured by a series of CD stopped-flow experiments in 100 mM Na^+ buffer at pH 7.0 and pH 5.5. Equimolar concentrations of SG1, potentially forming the G-quadruplex, and SC1, potentially forming the I-motif structure, were mixed. After rapid mixing of equal volumes of 50 μM SG1 solution and 50 μM SC1 solution, the self-associated structures, such as the G-quadruplex and the I-motif, started to be dissociated and then the unstructured SG1 and SC1 would form the Watson−Crick duplex. Comparing the CD spectra of the single-stranded SG1 and SC1 and the double-stranded SG1−SC1 in 100 mM Na^+ buffer at pH 7.0 with those at pH 5.5 (as shown in Figure S7 in the Supporting Information), it was reflected that the dynamic transition traces observed at the wavelength 295 nm for pH 7.0 and at the wavelength 288 nm for pH 5.5 would provide clearly the structural transitions that occurred in the cell after mixing. Although the G-quadruplex of SG1 had a typical band at 295 nm and the I-motif had a typical band at 288 nm at pH 5.5, the dynamic transition traces observed at 295 nm could reflect not only the unfolding of the G-quadruplex of SG1 for the mixing at pH 7.0 but also the association of the Watson−Crick duplex during the mixing. Similarly, both the unfolding of the I-motif of SC1 and the association of the duplex were reflected by the dynamic transition traces observed at 288 nm for the mixing at pH 5.5. In our stopped-flow experiments, dynamic transition traces were monitored by observing the CD intensity at the wavelengths corresponding to the typical bands of the G-quadruplex, the I-motif, and the duplex. The observed rates calculated from the time courses were proved to be independent of the monitored wavelength in every kinetic experiment (data not shown). Parts a and b, respectively, of Figure 7 show the kinetic traces in pH 7.0 and pH 5.5 buffer at 20 °C, as well as the corresponding fitting curves with a single-exponential function. The reaction at pH 7.0 rapidly reaches an equilibrium, that is, in less than 2000 s, whereas even after 3 h the time course shows that the reaction rate at pH 5.5 is still changing slowly. The observed rate at pH 7.0 was determined as $k_{obs}(7.0) = (8.06 \pm 0.4) \times 10^{-3}$ s^{-1}, while the observed rate at pH 5.5 was $k_{obs}(5.5) = (8.43 \pm 0.2) \times 10^{-4}$ s^{-1}.

The kinetic analysis provides insights into the mechanism of competition between the G-quadruplex, the I-motif, and

the WC duplex. The best fit to a single-exponential function for the data at pH 7.0 is consistent with eq 4, reflecting the dissociation of the SG1 G-quadruplex as the rate-limiting step for duplex formation in the mixture of SG1 and SC1. This is reasonable because of the fast association rate of the duplex and the unstable I-motif structure at pH 7.0 (*52*). For pH 5.5, the observed rate was only about one tenth of that at pH 7.0. The stability of the SC1 I-motif at pH 5.5 is comparable to that of the G-quadruplex SG1 (*40*), so that the dissociation rate of both the SG1 G-quadruplex and the SC1 I-motif might be very slow at pH 5.5. Additionally, a slow nucleation process induced by an electrostatic repulsion between the contiguous protonated cytosines, which is unfavorable for the formation of C^+·G base pairing (*53*), might be a reason for the slow reaction rate under acidic conditions. Recently, Phan and Mergny (*54*) presented a NMR study of duplex formation from the G-quadruplex $dAG_3(T_2AG_3)_3$ and the I-motif $d(C_3TA_2)_3C_3T$ that also showed a very low formation rate of the duplex—only a very small amount of the duplex formed after 26 h at pH 5.0 and 0 °C, although further investigation is still needed in order to explore in detail the mechanism of competition between the G-quadruplex, the I-motif, and the WC duplex.

We further investigated the temperature-dependency of the observed rate in the temperature range from 37 to 5 °C at both pH 7.0 and pH 5.5. Figure 7c shows the plots of ln k_{obs} versus the reciprocal of temperature. According to the Arrhenius equation, $k_{obs} = k_0 \exp(-E_a/RT)$, the apparent following activation energies E_a were determined: $E_a = 24.3$ kcal mol^{-1} K^{-1} at pH 7.0, and $E_a = 19.0$ kcal mol^{-1} K^{-1} at pH 5.5. As the temperature rose, the observed rate at pH 7.0 increased faster than that at pH 5.5. For example, at 37 °C, k_{obs}(7.0) was 0.0291 s^{-1}, while k_{obs}(5.5) was 0.00837 s^{-1}. The increase in the observed rates with the increase in temperature accords with the relationship of the dissociation rate of structured DNAs as a function of temperature; however, the difference between the apparent activation energy at pH 7.0 and that at pH 5.5 indicates that the I-motif indeed influences WC duplex formation in the mixture of the single-stranded structured DNAs.

Biological Implications. The results presented here imply that cation species, pH, and sequence context influence the structural competitive equilibria in the mixture of the G-quadruplex and the I-motif. The determinant effect of pH-dependent C-rich DNA sequences on the mechanism of structural competition points to a possible biological role for the I-motif in modulating DNA structures in vivo and may lead to the understanding of the intrinsic principles of molecular biological regulation in regard to the more acidic intracellular pH in cultured cancer or virus-transformed cells (*55*).

Our present investigation of the mechanism of structural competition between the G-quadruplex, the I-motif, and the duplex is also crucial for explaining the increasing number of reports that indicate that certain repetitive G-rich sequences adopt noncanonical base pairings, other than WC pairings, with their relevant complements. For instance, Hardin and co-workers (*27*) observed a reversible equilibrium between a Watson−Crick hairpin and a parallel intermolecular quadruplex. Miura and Thomas (*28*) and Deng and Braunlin (*29*) reported that a B-form duplex DNA was able to interconvert to intermolecular G-quadruplex structures under

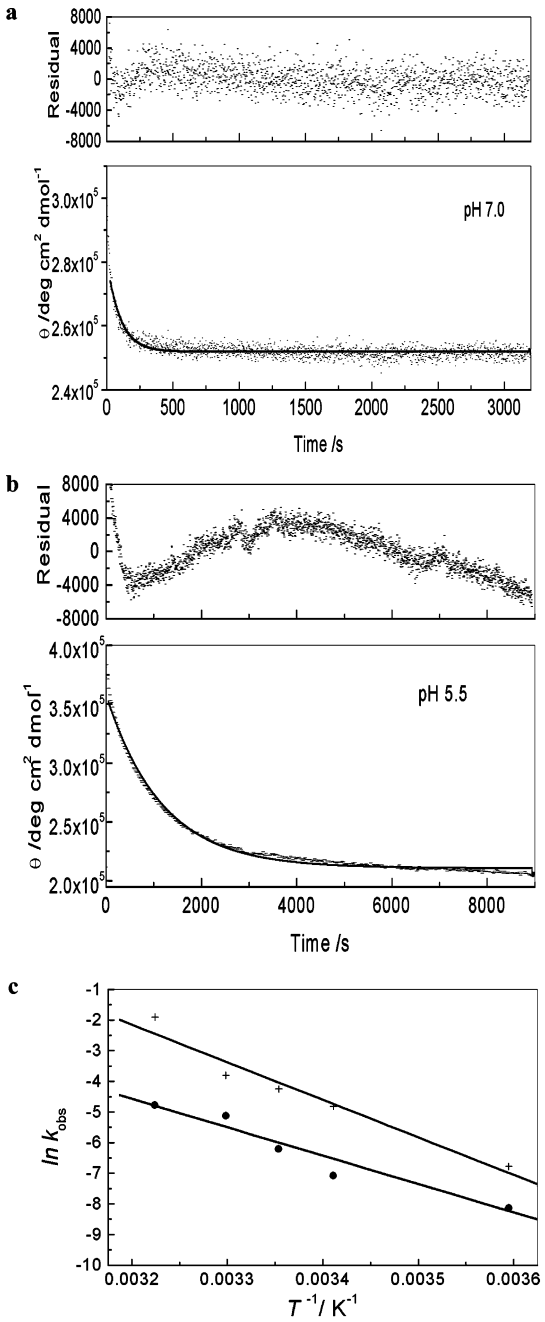

FIGURE 7: Kinetic time course obtained upon mixing equimolar concentrations of SG1 and SC1 in 100 mM Na^+ at 20 °C and (a) pH 7.0 or (b) pH 5.5. (a) The time courses at pH 7.0 were monitored at 295 nm (gray dots in the bottom panel). The solid line shows the best fit of the experimental data to a single-exponential function, giving $k_{obs} = (8.06 \pm 0.4) \times 10^{-3}$ s^{-1}. The residuals for the fit are shown as the black curve in the upper panel. (b) The time courses at pH 5.5 were monitored at 288 nm (gray dots in the bottom panel). The solid line shows the best fitting of the experimental data to a single-exponential function, giving $k_{obs} = (8.43 \pm 0.2) \times 10^{-4}$ s^{-1}. The residuals for the fit are shown with the black curve in the upper panel. (c) Plots of the observed rates vs the reciprocal of temperature at pH 7.0 (+) and pH 5.5 (●). In terms of the equation $k_{obs} = k_0 \exp(-E_a/RT)$, E_a values were determined as follows: $E_a = 24.3$ kcal mol^{-1} K^{-1} at pH 7.0, while $E_a = 19.0$ kcal mol^{-1} K^{-1} at pH 5.5.

certain cation concentrations. Manzini et al. (*30*) observed that quadruplex structures were stable enough to postpone or prevent the formation of the WC duplex in an equimolar mixture of $dAG_3(T_2AG_3)_3$ and $d(C_3TA_2)_3C_3T$ at acidic pH. Lacroix and Mergny (*31*) proved that the I-motif was a

competing structure for triplex formation at acidic pH. Ito et al. (*56*) reported a clear structural competition between the duplex and the G-quadruplex in the mixture dG_5T_5 and dA_5C_5. In addition, our data regarding the interaction between SG3 and the duplex SG1−SC1 are relevant for the proposed "t-loop" for telomere ends in mammalian cells, in which the telomeric duplex loops back on itself and the 3′-G strand extension displaces one strand of the duplex (*57*).

ACKNOWLEDGMENT

We greatly thank Ms. Kyoko Yasuda for her help in modifying the figures.

SUPPORTING INFORMATION AVAILABLE

Figures showing a typical ITC profile for the interaction between SG1 and SC1 in 100 mM Na^+ at pH 5.5 and 20 °C, native PAGE images, the effect of the duplex fraction on the values of thermodynamic parameters, CD spectra of the related three-strand systems, UV melting curves for these three-strand systems, plots of melting temperature against the species concentrations, the mobilities in the PAGE and the transition temperature, and CD spectra of the single-stranded SG1 and SC1 and the double-stranded SG1−SC1 in 100 mM Na^+ buffer at pH 7.0 and at pH 5.5, and text describing the effects of the duplex fraction on the values of thermodynamic parameters. This material is available free of charge via the Internet at http://pubs.acs.org.

REFERENCES

1. Paborsky, L. R., McCurdy, S. N., Griffin, L. C., Toole, J. J., and Leung, L. L. (1993) *J. Biol. Chem. 268*, 20808−20811.
2. Tasset, D. M., Kubik, M. F., and Steiner, W. (1997) *J. Mol. Biol. 272*, 688−698.
3. Sundquist, W. I., and Klug, A. (1989) *Nature 342*, 825−829.
4. Feigon, J., Dieckmann, T., and Smith, F. W. (1996) *Chem. Biol. 3*, 611−617.
5. Sen, D., and Gilbert, W. (1988) *Nature 334*, 364−366.
6. Mariappan, S. V., Catasti, P., Chen, X., Ratliff, R., Moyzis, R. K., Bradbury, E. M., and Gupta, G. (1996) *Nucleic Acids Res. 24*, 784−792.
7. Fry, M., and Loeb, L. A. (1994) *Proc. Natl. Acad. Sci. U.S.A. 91*, 4950−4954.
8. Murchie, A. T., and Lilley, D. M. (1992) *Nucleic Acids Res. 20*, 49−53.
9. Hammond-Kosack, M. C., Kilpatrick, M. W., and Docherty, K. (1992) *J. Mol. Endocrinol. 9*, 221−225.
10. Sundquist, W. I., and Heaphy, S. (1993) *Proc. Natl. Acad. Sci. U.S.A. 90*, 3393−3397.
11. Zahler, A. M., Williamson, J. R., Cech, T. R., and Prescott, D. M. (1991) *Nature 350*, 718−720.
12. Siddiqui-Jain, A., Grand, C. L., Bearss, D. J., and Hurley, L. H. (2002) *Proc. Natl. Acad. Sci. U.S.A. 99*, 11593−11598.
13. Arimondo, P. B. (2000) *Nucleic Acids Res. 28*, 4832−4838.
14. Sun, H., Karow, J. K., Hickson, I. D., and Maizels, N. (1998) *J. Biol. Chem. 273*, 27587−27592.
15. Fry, M., and Loeb, L. A. (1999) *J. Biol. Chem. 274*, 12797−127802.
16. Baran, N., Pucshanky, L., Marco, Y., Benjamin, S., and Manor, H. (1997) *Nucleic Acids Res. 25*, 297−303.
17. Neidle, S., and Read, M. A. (2000−2001) *Biopolymer 56*, 195−208.
18. Phan, A. T., Gueon, M., and Leroy, J. L. (2000) *J. Mol. Biol. 299*, 123−144.
19. Mergny, J. L., Lacroix, L. (1998) *Nucleic Acids Res. 26*, 4797−4803.
20. Cai, L., Raghavan, S., Ratliff, R., Mayzis, R., and Rich, A. (1998) *Nucleic Acids Res. 26*, 4696−4705.
21. Marsich, E., Xodo, L. E., and Manxini, G. (1998) *Eur. J. Biochem. 258*, 93−99.
22. Sun, D., Thompson, B., Cather, B. E., Salazar, M., Kerwin, S. M., Trent, J. O., Jenkins, T. C., Neidle, S., and Hurley, L. H. (1997) *J. Med. Chem. 40*, 2113−2116.
23. Wheelhouse, R. T., Sun, D., Han, H., Han, F. X., and Hurley, L. H. (1998) *J. Am. Chem. Soc. 120*, 3261−3262.
24. Rangan, A., Fedoroff, O. Y., and Hurley, L. H. (2001) *J. Biol. Chem. 276*, 4640−4646.
25. Alberti, P., Ren, J., Teulade-Fichou, M., Guittat, L., Riou, J. F., Chaires, J. B., Helene, C., Vigneron, J. P., Lehn, J. M., and Mergny, J. L. (2001) *J. Biomol. Struct. Dyn. 19*, 505−513.
26. Koeppel, F., Riou, J. F., Laoui, A., Mailliet, P., Arimonda, P., Labit, D., Petitgenet, O., Helene, C., and Mergy, J. L. (2001) *Nucleic Acids Res. 29*, 1087−1096.
27. Hardin, C. C., Corregan, M., Brown, B. A., and Frederick, L. N. (1993) *Biochemistry 32*, 5870−7880.
28. Miura, T., and Thomas, G. J. (1994) *Biochemistry 33*, 7848−7856.
29. Deng, H., and Braunlin, W. (1995) *Biopolymers 35*, 677−681.
30. Manzini, G., Yathindra, N., and Xodo, L. (1994) *Nucleic Acids Res. 22*, 4634−4640.
31. Lacroix, L., Mergny, J. L., and Helene, J. L. (1996) *Biochemistry 35*, 8715−8722.
32. Richards, E. G. (1975) in *Handbook of Biochemistry and Molecular Biology: Nucleic Acids* (Fasman, G. D., Ed.) 3rd ed., Vol. 1, pp 597−602, CRC Press, Cleveland, OH.
33. Miyoshi, D., Nakao, A., and Sugimoto, N. (2002) *Biochemistry 41*, 15017−15024.
34. Sugimoto, N., Nakano, S., Katoh, M., Matsumura, A., Nakamuta, H., Ohmichi, T., Yoneyama, M, and Sasaki, M. (1995) *Biochemistry 34*, 11211−11216.
35. Petersheim, M., and Turner, D. H. (1983) *Biochemistry 22*, 256−263.
36. Sugimoto, N., Nakano, M., and Nakano, S. (2000) *Biochemistry 39*, 11270−11281.
37. Marky, L. A., and Breslauer, K. J. (1987) *Biopolymers 26*, 1601−1620.
38. Wiseman, T., Williston, S., Brandts, J. F., and Lin, L. N. (1989) *Anal. Biochem. 179*, 131−137.
39. Moyzis, R. K., Buckingham, J. M., Cram, L. S., Dani, M., Deaven, L. L., Jones, M. D., Meyne, J., Ratliff, R. L., and Wu, J. R. (1988) *Proc. Natl. Acad. Sci. U.S.A. 85*, 6622−6626.
40. Li, W., Wu, P., Ohmichi, T., and Sugimoto, N. (2002) *FEBS Lett. 526*, 78−81.
41. Scaria, P. V., and Shafer, R. H. (1996) *Biochemistry 35*, 10985−10994.
42. Sugimoto, N., Wu, P., Hara, H., and Kawamoto, Y. (2001) *Biochemistry 40*, 9396−9405.
43. Miyoshi, D., Nakao, A., Toda, T., and Sugimoto, N. (2001) *FEBS Lett. 496*, 128−133.
44. Balagurumoorthy, P., Brahmachari, S., Mohanty, D., Bansal, M., and Sasisekharan, V. (1992) *Nucleic Acids Res. 20*, 4061−4067.
45. Balagurumoorthy, P., and Brahmachari, S. (1994) *J. Biol. Chem. 269*, 21858−21869.
46. Rippe, K., Fritsch, V., Westhof, E., and Jovin, T. (1992) *EMBO. J. 11*, 3777−3786.
47. Jing, N., Clercq, E., Rando, R., Pallansch, L., Lackman-Smith, C., Lee, S., Hogan, M. (2000) *J. Biol. Chem. 275*, 3421−3430.
48. Smirnov, I., and Shafer, R. H. (2000) *Biochemistry 39*, 1462−1468.
49. Hardin, C. C., Perry, A. G., and White, K. (2000−2001) *Biopolymers 56*, 147−194.
50. Simonsson, T. (2001) *Biol. Chem. 382*, 621−628.
51. Gowers, D. M., and Fox, K. R. (1999) *Nucleic Acids Res. 27*, 1569−1577.
52. Leroy, J. L., Gueron, M., Mergny, J. L., and Helence, C. (1994) *Nucleic Acids Res. 22*, 1600−1606.
53. Kiessling, L. L., and Dervan, P. B. (1992) *Biochemistry 31*, 2829−2834.
54. Phan, A. T., and Mergny, J. L. (2002) *Nucleic Acids Res. 30*, 4618−4625.
55. Gerson, D. F. (1978) in *Cell Cycle Regulation* (Jeter, J. R., Jr., Camerson, R., Padilla, G. M., and Zimmerman, A. M., Eds.) pp 105−130, Academic Press, Orlando, FL.
56. Ito, H., Tanaka, S., and Miyasaka, M. (2002) *Biopolymers 65*, 61−80.
57. Griffith, J. D., Comeau, L., Rosenfield, S., Stansel, R. M., Bianchi, A., Moss, H., and de Lange, T. (1999) *Cell 97*, 503−514.

BI034168J